

# The air pressure effect on the homogeneous nucleation of carbon dioxide by molecular simulation

M. Horsch<sup>a</sup>, Z. Lin<sup>a,1</sup>, T. Windmann<sup>a</sup>, H. Hasse<sup>b</sup>, J. Vrabec<sup>a,\*</sup>

<sup>a</sup>Universität Paderborn, Lehrstuhl für Thermodynamik und Energietechnik, Warburger Str. 100, 33098 Paderborn, Germany

<sup>b</sup>Technische Universität Kaiserslautern, Lehrstuhl für Thermodynamik, Erwin-Schrödinger-Str. 44, 67663 Kaiserslautern, Germany

---

## Abstract

Vapour-liquid equilibria (VLE) and the influence of an inert carrier gas on homogeneous vapour to liquid nucleation are investigated by molecular simulation for quaternary mixtures of carbon dioxide, nitrogen, oxygen, and argon. Canonical ensemble molecular dynamics simulation using the Yasuoka-Matsumoto method is applied to nucleation in supersaturated vapours that contain more carbon dioxide than in the saturated state at the dew line. Established molecular models are employed that are known to accurately reproduce the VLE of the pure fluids as well as their binary and ternary mixtures. On the basis of these models, also the quaternary VLE properties of the bulk fluid are determined with the Grand Equilibrium method.

Simulation results for the carrier gas influence on the nucleation rate are compared with the classical nucleation theory (CNT) considering the ‘pressure effect’ [Phys. Rev. Lett. 101: 125703 (2008)]. It is found that the presence of air as a carrier gas decreases the nucleation rate only slightly and, in particular, to a significantly lower extent than predicted by CNT. The nucleation rate of carbon dioxide is generally underestimated by CNT, leading to a deviation between one and two orders of magnitude for pure carbon dioxide in the vicinity of the spinodal line and up to three orders of magnitude in presence of air as a carrier gas. Furthermore, CNT predicts a temperature dependence of the nucleation rate in the spinodal limit, which cannot be confirmed by molecular simulation.

**Keywords:** homogeneous nucleation, carrier gas, pressure effect, molecular dynamics

**PACS:** 64.60.Ej, 05.70.Np, 36.40.-c

---

---

\*Author to whom correspondence should be addressed: Jadran Vrabec, Universität Paderborn, Institut für Verfahrenstechnik, Lehrstuhl für Thermodynamik und Energietechnik, +49 5251 60 2421 (phone), +49 5251 60 3522 (fax).

*Email address:* jadran.vrabec@upb.de (J. Vrabec)

*URL:* <http://thet.upb.de/> (J. Vrabec)

<sup>1</sup>蔺增勇 (Lin Zengyong)

## 1. Introduction

If significant reductions in greenhouse gas emissions are to be achieved, it is essential to minimize the energy required for separating carbon dioxide from air as a prerequisite for rendering purification, recovery and sequestration processes economically and ecologically more efficient (Kaule, 2002). This requires an accurate understanding of the phase behaviour of carbon dioxide (CO<sub>2</sub>) in the earth's atmosphere under diverse conditions, corresponding to the respective technical applications.

Condensation processes, initiated by nucleation, as well as vapour-liquid equilibria (VLE) are particularly relevant in this context, since they characterize capture and storage of CO<sub>2</sub>, i.e. phase separation and phase equilibrium. The present study concentrates on understanding homogeneous nucleation and VLE properties for quaternary mixtures consisting of CO<sub>2</sub>, nitrogen (N<sub>2</sub>), oxygen (O<sub>2</sub>), and argon (Ar) by means of molecular simulation. Thereby, the properties of the investigated fluid itself can be fully isolated from phenomena induced by impurities or boundary effects in the vicinity of a solid wall, which would be much harder to accomplish in an experimental arrangement.

Although a systematic discussion of CO<sub>2</sub> nucleation was, surprisingly enough, published for the ambient conditions prevailing on Mars (Määttä et al., 2005), to the authors' knowledge no analogous study is available for the ecologically and technically more relevant atmosphere composition of our own planet. The present work closes this gap and characterizes the air pressure effect on the condensation process in a vapour containing more CO<sub>2</sub> than at saturation on the basis of molecular models that are known to accurately reproduce VLE properties.

Direct MD simulation of nucleation in the canonical ensemble with the Yasuoka-Matsumoto (YM) method is an established approach (Yasuoka and Matsumoto, 1998, Matsubara et al., 2007). According to that approach, the nucleation rate is approximated by the frequency at which sufficiently large droplets emerge in the simulated volume. The YM method can be successfully applied to the regime where the supersaturation is sufficiently high to permit significant droplet formation in a nanoscopic volume within a few nanoseconds, but not as high that the nucleation rate  $j$  is affected by depletion of the vapour due to droplet formation within the same time interval (Horsch et al., 2008a,b, Chkonia et al., 2009). Lower nucleation rates can be determined by forward flux sampling or methods based on umbrella sampling (Valeriani et al., 2005), whereas in the immediate vicinity of the spinodal line, where the metastable state would otherwise break down, a stationary value for the nucleation rate can be obtained by grand canonical MD simulation with McDonald's daemon (Horsch and Vrabec, 2009).

The present work focuses on the intermediate regime, where the YM method is viable, and compares simulation results with theoretical predictions on the basis of two variants of the classical nucleation theory (CNT).

## 2. The pressure effect

If the pressure effect (PE) is taken into account, the free energy  $G$  of formation according to CNT is given by (Wedekind et al., 2008)

$$dG_{\text{PE}} = \left( \mu_s - \mu - \frac{\mathcal{P}_s - p}{\rho'} \right) dN + \gamma dF, \quad (1)$$

for a droplet containing  $\mathcal{N}$  molecules, whereas the more commonly used – but thermodynamically inconsistent – simplified classical (SC) variant of CNT implies

$$dG_{\text{SC}} = (\mu_s - \mu) d\mathcal{N} + \gamma dF. \quad (2)$$

Therein,  $\mu_s$  and  $\mathcal{P}_s$  as well as  $\mu$  and  $p$  represent the saturated and supersaturated values of chemical potential and pressure, respectively. While  $\mathcal{P}_s$  refers to the pure substance vapour pressure of the nucleating component,  $p$  is the total pressure including the pressure contribution of an inert carrier gas, if present. The droplet surface tension is given by  $\gamma$ , the area of the surface of tension is  $F$ , and  $\rho'$  represents the density of the liquid which is assumed to be incompressible. Where the chemical potential difference  $\Delta\mu = \mu - \mu_s$  appears in the SC expression, PE applies an ‘effective’ difference (Wedekind et al., 2008)

$$\Delta\mu_e = \Delta\mu + \frac{\mathcal{P}_s - p}{\rho'}, \quad (3)$$

which is always smaller than  $\Delta\mu$ . Assuming a spherical shape for the emerging droplets, i.e.

$$dF = \left( \frac{32\pi}{3\rho'^2 \mathcal{N}} \right)^{1/3} d\mathcal{N}, \quad (4)$$

and neglecting the curvature dependence of the surface tension, the free energy barrier of the nucleation process according to the PE variant of CNT

$$\Delta G_{\text{PE}}^* = \frac{16\pi\gamma_0^3}{3(\rho'\Delta\mu_e)^2} + \Delta\mu_e - \pi^{1/3} \left( \frac{6}{\rho'} \right)^{2/3} \gamma_0, \quad (5)$$

is reached for the critical droplet size

$$\mathcal{N}_{\text{PE}}^* = \frac{32\pi}{3\rho'^2} \left( \frac{\gamma_0}{\Delta\mu_e} \right)^3. \quad (6)$$

These expressions use the surface tension  $\gamma_0$  of the planar vapour-liquid interface as well as the ‘internally consistent’ approach of Blander and Katz (1972) which equates single-molecule droplets with vapour monomers and assigns them a free energy of formation  $\Delta G = 0$ . The same results follow for the SC variant, with  $\Delta\mu$  instead of  $\Delta\mu_e$  in Eqs. (5) and (6).

The long-term growth probability  $Q(M)$  of a droplet containing  $M$  molecules can be given by

$$Q(M) = \int_1^M \exp\left(\frac{2\Delta G(\mathcal{N})}{kT}\right) d\mathcal{N} \left[ \int_1^\infty \exp\left(\frac{2\Delta G(\mathcal{N})}{kT}\right) d\mathcal{N} \right]^{-1}, \quad (7)$$

under the approximation that the reaction coordinate of the nucleation process only depends on the droplet size  $\mathcal{N}$ , based on the analysis of a random walk over a single discrete order parameter (Horsch et al., 2009). It should be noted that  $Q(M)$  is extremely small for values of  $M$  significantly below the critical droplet size and converges to 1 as  $M$  increases. The transition rate of vapour monomers of the nucleating component through an interface, normalized by the surface area of the interface, is

$$\beta = \mathcal{P} (2\pi m_0 kT)^{-1/2}, \quad (8)$$

according to kinetic gas theory, where  $k$  is the Boltzmann constant,  $m_0$  is the molecular mass and  $\mathcal{P}$  the pressure of the nucleating component in its pure gaseous state at the same partial density. The isothermal nucleation rate according to CNT is (Feder et al., 1966)

$$j_T = ZF^* \beta \tilde{\rho} \exp\left(\frac{-\Delta G^*}{kT}\right), \quad (9)$$

which depends on the surface area  $F^*$  of the critical droplet, the Zěl'dovič (1942) factor

$$Z = \left(\frac{-d^2G/dN^2}{2\pi m_0 kT}\right)_{N=N^*}^{1/2}, \quad (10)$$

as well as the density of vapour monomers belonging to the nucleating component  $\tilde{\rho}$ . Droplet overheating due to rapid growth, however, is neglected in the expression for  $j_T$ .

Even slightly below the spinodal supersaturation, most of the molecules of the nucleating component belong either to the vapor phase (i.e. they are monomers) or to clusters of ten or less molecules, during the regime of a condensation process that is dominated by nucleation. For the metastable quasi-equilibrium that prevails within this regime, the Boltzmann distribution applies. The monomer density in the metastable state is therefore given by

$$\rho Y_0 = \tilde{\rho} \sum_{N=1}^{N^*} N \exp\left(\frac{-\Delta G(N)}{kT}\right), \quad (11)$$

a series that usually converges very fast, wherein  $\rho$  is the total density of the supersaturated vapour and  $Y_0$  is the mole fraction of the nucleating component in the supersaturated vapour. The presence of droplets above the critical size, which is not accounted for by Eq. (11), can be neglected during nucleation, since a significant amount of large droplets would imply that the vapour phase is depleted to a considerable extent, so that droplet growth instead of nucleation would be the predominant phenomenon.

The presence of a carrier gas also influences the thermalization of growing droplets, facilitating the heat transfer from the liquid to the surrounding vapour and thereby decreasing the amount of overheating. The coupling between heat and mass transfer from the metastable to the dispersed phase during nucleation was first consistently analyzed by Feder et al. (1966) who considered a diffusion process over the two most relevant order parameters, droplet size  $N$  and temperature  $T$ . The overall heat transfer effect on the nucleation rate is covered by the thermal non-accomodation prefactor (Feder et al., 1966)

$$j = \frac{b^2}{b^2 + q^2} j_T. \quad (12)$$

Therein,

$$q = h'' - h' - \frac{kT}{2} - \gamma \left(\frac{dF}{dN}\right)_{N=N^*}, \quad (13)$$

is the enthalpy added to a droplet when it absorbs a molecule of the nucleating component from the vapour (Feder et al., 1966) and

$$b^2 = kT^2 \left(c_{v,0} + \frac{k}{2}\right) \sum_{i=0}^K \frac{Y_i m_0^{1/2} (c_{v,i} + k/2)}{Y_0 m_i^{1/2} (c_{v,0} + k/2)}, \quad (14)$$

is the mean square fluctuation of the kinetic energy for the vapour molecules (Feder et al., 1966, Wedekind et al., 2008) and quantifies the thermalization effect of the vapor. Furthermore,  $h'$  and  $h''$  are the saturated liquid and vapour enthalpy, respectively, and  $c_{v,i}$  is the isochoric heat capacity of component  $i$  where  $i = 0$  stands for the nucleating component and  $1 \leq i \leq K$  the components of the inert carrier gas. Within the scope of the present study, the heat capacity of the pure saturated vapour is used for  $c_{v,0}$  whereas for the other  $c_{v,i}$  the value in the limit of infinite dilution is used, since CNT assumes the carrier gas to have ideal properties (Wedekind et al., 2008).

Within the framework of CNT, it follows that the prefactor

$$ZF^* = \frac{2}{\rho'} \left( \frac{\gamma_0}{kT} \right)^{1/2}, \quad (15)$$

does not depend on the pressure contribution of the carrier gas, and neither does  $\beta$ , while the influence of the carrier gas pressure on  $\tilde{\rho}$ , which is usually similar in magnitude to  $\rho Y_0$ , is of minor significance. This eliminates all contributions to the pressure effect except for those discussed by Wedekind et al. (2008) as

$$\frac{j_{\text{PE}}}{j_{T,\text{SC}}} = \frac{b_{\text{PE}}^2}{b_{\text{PE}}^2 + q_{\text{PE}}^2} \frac{j_{T,\text{PE}}}{j_{T,\text{SC}}}. \quad (16)$$

Normalized to unity for the pure fluid ( $Y_0 = 1$ ) with the PE variant of CNT, the Wedekind et al. (2008) pressure effect can be expressed as

$$\mathcal{W}(Y_0) = \frac{b_{\text{PE}}^2(Y_0) [b_{\text{PE}}^2(Y_0 = 1) + q_{\text{PE}}^2(Y_0 = 1)]}{[b_{\text{PE}}^2(Y_0) + q_{\text{PE}}^2(Y_0)] b_{\text{PE}}^2(Y_0 = 1)} \exp\left(\frac{\Delta G_{\text{PE}}^*(Y_0 = 1) - \Delta G_{\text{PE}}^*(Y_0)}{kT}\right), \quad (17)$$

given that  $j_{T,\text{SC}}$ , the denominator of Eq. (16), does not depend on  $Y_0$ .

Under certain conditions, the pressure effect does not exceed the experimental uncertainty and can thus be neglected (Iland et al., 2004). In other cases, however, the influence can be experimentally detected, with apparently contradictory results: sometimes  $j$  increases with the amount of carrier gas, in other cases the opposite tendency is observed (Hyvärinen et al., 2006, Brus et al., 2008). The  $\mathcal{W}$  factor explains this in principle, since it combines the thermal non-accommodation factor, which increases with  $Y_0 \rightarrow 0$ , and the free energy effect that leads to an effective chemical potential difference  $\Delta\mu_e < \Delta\mu$ . Depending on the thermodynamic conditions, each of these contributions can be predominant (Wedekind et al., 2008).

The main inaccuracies of CNT concern the surface tension as well as the droplet surface area. For the surface tension, deviations from the capillarity approximation  $\gamma \approx \gamma_0$  are known to occur for nanoscopically curved interfaces (Moody and Attard, 2003, Szybisz and Urrutia, 2003, Horsch et al., 2008b). The Tolman (1949) approach implies huge deviations from  $\gamma_0$  for droplets on the molecular length scale corresponding to the Tolman length  $\delta$ . In particular, for  $\mathcal{R}_\gamma > \delta$  the dependence of  $\gamma$  on the surface of tension radius  $\mathcal{R}_\gamma$  can be expressed as

$$\gamma = \gamma_0 \exp\left[-2\left(\frac{\delta}{\mathcal{R}_\gamma}\right) + \left(\frac{\delta}{\mathcal{R}_\gamma}\right)^2 - \frac{2}{9}\left(\frac{\delta}{\mathcal{R}_\gamma}\right)^3 + O\left([\delta/\mathcal{R}_\gamma]^4\right)\right], \quad (18)$$

whereas  $\gamma \sim \mathcal{R}_\gamma$  becomes valid for  $\mathcal{R}_\gamma \ll \delta$ . From the Laplace equation along with the Tolman (1949) approach it can be deduced that the area of the surface of tension is given by

$$dF = \frac{2dN}{\mathcal{R}_\gamma \rho'}, \quad (19)$$

for an incompressible fluid, where the relation

$$\mathcal{R}_\gamma = \left( \frac{3N}{4\pi\rho'} \right)^{1/3} - \delta, \quad (20)$$

follows for the dependence of the surface of tension radius on  $N$ . Overall, this leads to a significantly increased surface area for droplets on the molecular length scale.

### 3. Simulation methods and models

The evaluation of the theoretical predictions relies on knowledge about the chemical potential difference between the saturated and the supersaturated state. This was obtained for pure CO<sub>2</sub> by Gibbs-Duhem integration

$$\Delta\mu(T, p) = \int_{p_s(T)}^p \frac{dp}{\rho(T, p)}, \quad (21)$$

using MD simulation results of small systems ( $N \approx 10\,000$ ) in the metastable vapour regime. The carrier gas influence according to the presented variants of CNT was evaluated by assuming ideal gas properties for air as well as ideal mixing behaviour, i.e.

$$p = (1 - Y_0)\rho kT + \mathcal{P}. \quad (22)$$

The total number of molecules was up to  $N = 900\,000$  such that the carrier gas with  $N(\text{N}_2) : N(\text{O}_2) : N(\text{Ar}) = 7812 : 2095 : 93$  corresponded to the earth's atmosphere composition. All simulations were conducted with the *ls1 mardyn* molecular dynamics program (Bernreuther et al., 2009), employing the Verlet leapfrog algorithm with an integration time step of 2 fs. The temperature was regulated by velocity rescaling. Note that the influence of the overall momentum of the system on its effective temperature can be neglected due to the large number of particles.

For the homogeneous nucleation simulations, the YM method was applied to relatively large, but still nanoscopic systems with  $N(\text{CO}_2) = 300\,000$ . The condensation process is thereby regarded as a succession of three characteristic stages: relaxation, nucleation, and droplet growth (Chesnokov and Krasnoperov, 2007). Attention was paid to cover the regime dominated by nucleation over a sufficient time span to obtain statistically significant results, which required a simulated time between a few hundred picoseconds and a few nanoseconds, depending on the nucleation rate.

During the nucleation stage, the droplet formation rate  $I(M)$ , i.e. the number of droplets containing at least  $M$  molecules formed over time, is approximately constant (Yasuoka and Matsumoto, 1998). The droplet formation rate depends on the threshold size  $M$  and is related to the nucleation rate by

$$\frac{I(M)}{V} = \frac{j}{Q(M)}, \quad (23)$$

since  $Q(M)$  indicates the probability for a droplet containing  $M$  molecules to reach macroscopic size.

Liquid and vapour were distinguished according to the Stillinger (1963) criterion with a connectivity radius of 5.08 Å: following this approach, all molecules with a neighbor at a distance below the connectivity radius were considered as belonging to the liquid phase, so that the vapor phase only consisted of molecules where no such neighbor was present. A graph was constructed with each node representing a molecule of the liquid phase, containing edges between those molecules with a distance below the connectivity radius. The biconnected components of that graph, determined by the algorithm of Hopcroft and Tarjan (1973) such that any single connection can be eliminated without disrupting the internal connectivity, were defined to be liquid droplets.

Fluid argon can be represented by the Lennard-Jones (LJ) potential

$$u_{\text{LJ}}(r) = 4\varepsilon \left[ \left( \frac{\sigma}{r} \right)^{12} - \left( \frac{\sigma}{r} \right)^6 \right], \quad (24)$$

in dependence of the interatomic distance  $r$ . Molecular models for CO<sub>2</sub>, N<sub>2</sub> as well as O<sub>2</sub>, which can be represented by two LJ sites separated by the constant elongation  $\ell$  with a superimposed quadrupole moment  $Q$  in the molecule's centre of mass (2CLJQ), yielding (Vrabec et al., 2001)

$$u(\mathbf{r}, \omega_1, \omega_2) = f(\omega_1, \omega_2) Q^2 |\mathbf{r}|^{-5} + \sum_{s_{1,2} \in \{-1,1\}} u_{\text{LJ}} \left( \left| \mathbf{r} + \sum_{n=1}^2 \frac{s_n \ell_n \omega_n}{2} \right| \right), \quad (25)$$

were adjusted to pure fluid VLE data by Vrabec et al. (2001), cf. Tab. 1. Therein,  $\mathbf{r}$  is the distance between the centers of mass of the two interacting 2CLJQ molecules, and the function  $f(\omega_1, \omega_2)$  only depends on their orientation as expressed by the unit vectors  $\omega_1$  and  $\omega_2$ , respectively (Gray and Gubbins, 1984, Vrabec et al., 2001). If adequate values for the unlike dispersive interaction energy are used, so that binary VLE are reproduced correctly (Vrabec et al., 2009a), cf. Fig. 1, ternary mixtures are accurately described without any further adjustment (Huang et al., 2009). In Tab. 1, the unlike energy parameters are indicated in terms of the binary interaction parameter  $\xi$  of the modified Berthelot (1898) combining rule (Schnabel et al., 2007b)

$$\varepsilon_{\text{AB}} = \xi(\varepsilon_{\text{A}}\varepsilon_{\text{B}})^{1/2}, \quad (26)$$

while the unlike LJ size parameter is determined as an arithmetic mean according to the Lorentz (1881) combining rule. This approach has also been validated with an emphasis on CO<sub>2</sub> in particular, confirming its viability for mixtures with N<sub>2</sub> and O<sub>2</sub> (Vrabec et al., 2009b) as well as hydrogen bonding fluids (Schnabel et al., 2007a).

On that basis, quaternary phase equilibria were determined using the Grand Equilibrium method (Vrabec and Hasse, 2002), introducing Ar into the system studied by Vrabec et al. (2009b). The Grand Equilibrium method calculates the vapour pressure  $p_s$  as well as all dew line mole fractions  $y_i$  by simulation for a specified temperature  $T$  and a specified bubble line (i.e., saturated bulk liquid) mole fraction  $x_i$  for all components of the mixture. Although no experimental data are available for the quaternary mixture, the simulation results can be trusted due to the extensive

	type	$\sigma$ [Å]	$\varepsilon$ [meV]	$\ell$ [Å]	$Q$ [ $e\text{Å}^2$ ]	$\xi$ (Ar)	$\xi$ (O <sub>2</sub> )	$\xi$ (N <sub>2</sub> )
CO <sub>2</sub>	2CLJQ	2.9847	11.394	2.418	0.78985	0.999	0.979	1.041
N <sub>2</sub>	2CLJQ	3.3211	3.0072	1.046	0.29974	1.008	1.007	
O <sub>2</sub>	2CLJQ	3.1062	3.7212	0.9699	0.16824	0.988		
Ar	LJ	3.3967	10.087					

Table 1: Molecular model parameters of Vrabec et al. (2001), i.e. the size parameter  $\sigma$  and the energy parameter  $\varepsilon$  for the LJ interaction sites as well as the molecular elongation  $\ell$  and the quadrupole moment  $Q$  associated with the 2CLJQ models. The binary interaction parameters  $\xi$  shown in the Table were adjusted to binary VLE data by Vrabec et al. (2009a).

validation of the models with respect to the VLE behaviour for all of the six binary (Vrabec et al., 2009a) and two of the four ternary subsystems (Huang et al., 2009), i.e. N<sub>2</sub> + O<sub>2</sub> + Ar as well as CO<sub>2</sub> + N<sub>2</sub> + O<sub>2</sub>.

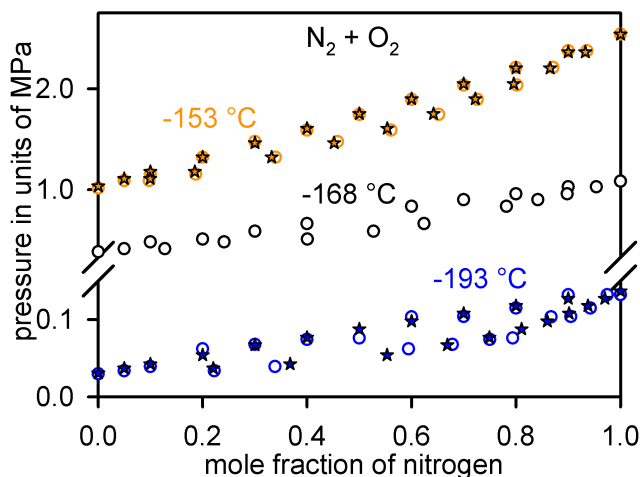


Figure 1: (Colour on the web, b/w in print.) Experimental data ( $\star$ ) of Dodge (1927) and simulation results ( $\circ$ ) of Vrabec et al. (2009a), using the Grand Equilibrium method with the molecular models given in Tab. 1, for VLE of binary mixtures containing nitrogen and oxygen at temperatures of  $T = -193$ ,  $-168$ , and  $-153$  °C.

#### 4. Simulation results

Grand Equilibrium simulations of the quaternary mixture CO<sub>2</sub> + N<sub>2</sub> + O<sub>2</sub> + Ar were conducted for VLE covering a broad temperature range with CO<sub>2</sub> bubble line mole fractions  $x(\text{CO}_2)$  of 0.910, 0.941, and 0.969, cf. Tab. 2. Except for the highest temperature, corresponding to 93.0 % of the critical temperature for pure CO<sub>2</sub> which is  $T_c(\text{CO}_2) = 314.18 \pm 0.04$  K according to Suehiro et al. (1996), the mole fractions  $y(\text{N}_2)$ ,  $y(\text{O}_2)$ , and  $y(\text{Ar})$  on the dew line are one order of magnitude higher than the corresponding bubble line mole fractions. This confirms that for temperatures sufficiently below  $T_c(\text{CO}_2)$ , air only accumulates to a limited extent in the liquid phase. As a first approximation, it can therefore be treated as a carrier gas for CO<sub>2</sub> nucleation so that the PE variant of CNT with a single nucleating component can be applied, as opposed to more complex

mixtures such as ethanol + hexanol (Strey and Viisanen, 1993), water-alcohol mixtures (Viisanen et al., 1994, Strey et al., 1995), or water + nonane + butanol (Nellas et al., 2007), where multi-component nucleation occurs.

From MD simulation of small metastable systems, the spinodal value  $S^\nabla$  of the supersaturation with respect to density, which is defined as

$$S = \frac{\rho Y_0}{\rho''(T)}, \quad (27)$$

wherein  $\rho''(T)$  is the saturated vapour density of pure  $\text{CO}_2$ , was determined to be in the range  $4.3 \leq S^\nabla \leq 5.1$  at  $-44.8^\circ\text{C}$ ,  $3.6 \leq S^\nabla \leq 4.3$  at  $-34.8^\circ\text{C}$ , and  $3.0 \leq S^\nabla \leq 3.6$  at  $-23^\circ\text{C}$  for  $Y_0 = 1$ . At these temperatures, canonical ensemble MD simulations for  $\text{CO}_2$  nucleation were conducted using the YM method with  $\text{CO}_2$  mole fractions of 1/3, 1/2, and 1 at supersaturations below the spinodal value  $S^\nabla$ , but still high enough to obtain statistically reliable droplet formation rates in a nanoscopic volume on the timescale of a few nanoseconds.

YM droplet formation rates  $I$  from the present work as well as a previous study (Horsch et al., 2008a) are shown in Fig. 2 for  $Y_0 = 1$ , i.e. pure  $\text{CO}_2$ . The dependence of  $I$  on the threshold size  $M$  reproduces the typical picture: for low threshold sizes (probably smaller than  $N^*$ ) the droplet formation rate can be elevated by several orders of magnitude, and it converges for  $M \gg N^*$  under the condition that the depletion of the vapour can be neglected (Yasuoka and Matsumoto, 1998). For very large values of  $M$  – not shown in Fig. 2 – the droplet formation rate decreases again, because the presence of many large droplets implies that a substantial amount of the vapour monomers have already been consumed by the emerging liquid phase.

The pressure effect in the pure fluid, expressed by  $j_{\text{SC}}/j_{\text{PE}}$ , was found to be most significant at high temperatures, partly because this coincides with a lower density of the liquid, but also because  $\Delta\mu$  is smaller so that the relative deviation between  $\Delta\mu_c$  and  $\Delta\mu$  is increased. The most striking observation is that while both variants of CNT predict the value of  $j$  in the spinodal limit to increase with temperature – mainly because  $T$  occurs in the denominator of the exponential in the Arrhenius term of Eq. (9) – the simulation results do not exhibit any significant temperature

$T$ [ $^\circ\text{C}$ ]	$x(\text{CO}_2)$	$p_s$ [MPa]	$y/x(\text{N}_2)$	$y/x(\text{O}_2)$	$y/x(\text{Ar})$	$\rho'$ [mol/l]	$\rho''$ [mol/l]	$h'' - h'$ [kJ/mol]
-90.3	0.969	2.53(8)	40(2)	24.5(9)	24.7(9)	29.24(1)	1.854(2)	17.092(9)
	0.941	3.9(1)	21.5(8)	13.9(5)	13.7(5)	29.13(1)	3.031(5)	16.27(1)
	0.910	6.0(2)	13.7(4)	9.1(3)	9.0(3)	29.01(2)	5.29(2)	15.12(1)
-40.3	0.941	4.38(5)	14.0(2)	10.8(1)	10.3(1)	24.94(3)	2.663(5)	13.30(1)
	0.910	5.30(4)	9.7(1)	7.72(8)	7.34(8)	24.47(2)	3.247(7)	12.64(1)
9.7	0.969	5.97(4)	5.6(1)	4.88(8)	4.72(7)	19.3(2)	3.90(1)	8.55(5)
	0.941	6.98(3)	4.31(5)	3.82(5)	3.67(4)	18.55(9)	4.63(2)	7.79(4)

Table 2: VLE data for the quaternary system  $\text{CO}_2 + \text{N}_2 + \text{O}_2 + \text{Ar}$ , including the temperature  $T$ , the saturated vapor pressure  $p_s$ , the saturated bulk densities of the liquid and the vapor phase, i.e.  $\rho'$  and  $\rho''$ , respectively, as well as the vaporization enthalpy  $h'' - h'$ . The saturated bulk liquid composition was specified to be equimolar in nitrogen, oxygen, and argon, i.e.  $x(\text{N}_2) = x(\text{O}_2) = x(\text{Ar}) = [1 - x(\text{CO}_2)] / 3$ , and the dew line mole fractions  $y$  indicated in the table are reduced by the bubble line mole fractions of the respective components. Values in parentheses indicate the uncertainty in terms of the last given digit.

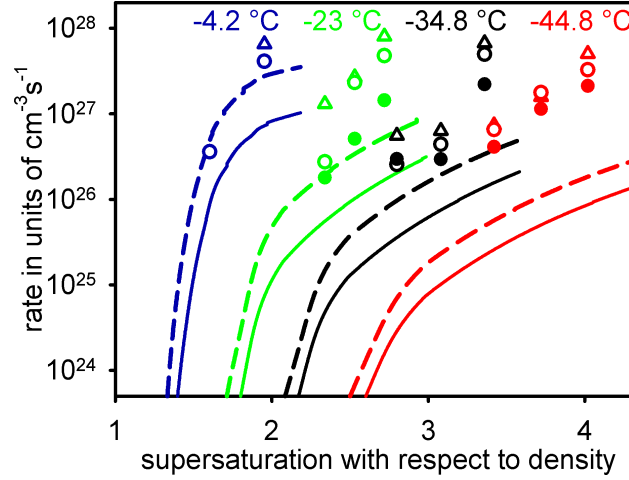


Figure 2: (Colour on the web and in print.) Pure CO<sub>2</sub> nucleation rate  $j$  according to the PE (—) and SC (---) variants of CNT in comparison to  $I/V$  for threshold sizes of  $M = (\Delta)$  50,  $(\circ)$  75, and 250  $(\bullet)$  molecules from canonical ensemble MD simulation over supersaturation  $S = \rho/\rho''(T)$  at temperatures of  $T = -44.8, -34.8, -23,$  and  $-4.2$  °C. The simulation results for  $T = -4.2$  °C are taken from previous work and were obtained using a different cluster criterion (Horsch et al., 2008a).

dependence for the attainable value of  $j$ . In the spinodal limit, the nucleation rate appears to be about  $j(T, S^\nabla) \approx 10^{27} \text{ cm}^{-3} \text{ s}^{-1}$  over the whole temperature range.

This deviation between CNT and the simulation results may be due to a qualitative discrepancy concerning the magnitude of the free energy barrier  $\Delta G^*$  in the spinodal limit. The spontaneous collapse of unstable states implies that the free energy barrier converges to zero in the spinodal limit, which does not necessarily mean that the critical droplet size converges to zero as well (Wedekind et al., 2009). However, this effect is not reproduced by CNT where a non-zero value of  $\Delta G^*$  is obtained for arbitrary magnitudes of the supersaturation, including  $S^\nabla$ . Since  $\Delta G^*$  is divided by the temperature due to the Arrhenius approach, this effect is bound to be more significant at lower temperatures.

Table 3 indicates the results for the carrier gas effect on CO<sub>2</sub> nucleation at  $T = -44.8$  °C. As usual,  $I$  decreases when larger values of the threshold size  $M$  are regarded, but it can also be seen that this effect is clearly stronger when more air is present in the system. This leads to values for the overall carrier gas effect  $\mathcal{G}$  on the droplet formation rate

$$\mathcal{G} = \frac{I(S, Y_0, M)}{I(S, Y_0 = 1, M)}, \quad (28)$$

that are greater than unity for relatively small values of  $M$ , but converge to values significantly below unity as  $M$  is increased. This result can be understood if the carrier gas effect on  $\mathcal{N}^*$  according to Eqs. (3) and (6) is considered: with a higher total pressure,  $\Delta\mu_e$  decreases which affects the critical droplet size to the third power, leading to significantly larger values of  $\mathcal{N}_{\text{PE}}^*$ , cf. Tab. 3. Thus, for relatively small threshold sizes, the long-term growth probability is significantly smaller, cf. Eq. (7), which in turn increases the droplet formation rate according to Eq. (23). Hence, the apparently contradictory values of  $\mathcal{G}$  are actually consistent and correspond to a negative dependence

$S$	$Y_0$	$M$	$I/V$ [ $\text{cm}^{-3}\text{s}^{-1}$ ]	$\mathcal{G}$	$\mathcal{N}_{\text{PE}}^*$	$\mathcal{W}$	$j_{\text{PE}}$ [ $\text{cm}^{-3}\text{s}^{-1}$ ]	$j/Q_{\text{PE}}$ [ $\text{cm}^{-3}\text{s}^{-1}$ ]
3.42	1/3	50	$2.7 \times 10^{27}$	3.6	61	$8.5 \times 10^{-3}$	$5.2 \times 10^{23}$	$3.0 \times 10^{24}$
		75	$5.2 \times 10^{26}$	0.79				$6.1 \times 10^{23}$
		85	$3.8 \times 10^{26}$	0.63				$5.4 \times 10^{23}$
	1/2	50	$1.1 \times 10^{27}$	1.5	44	0.17	$9.8 \times 10^{24}$	$1.4 \times 10^{25}$
		75	$3.1 \times 10^{26}$	0.47				$9.8 \times 10^{24}$
		85	$2.4 \times 10^{26}$	0.39				$9.8 \times 10^{24}$
	1	50	$7.3 \times 10^{26}$	1	33	1	$5.0 \times 10^{25}$	$5.2 \times 10^{25}$
		75	$6.5 \times 10^{26}$	1				$5.0 \times 10^{25}$
		85	$6.1 \times 10^{26}$	1				$5.0 \times 10^{25}$
3.72	1/3	50	$1.4 \times 10^{28}$	8.7	61	$5.8 \times 10^{-3}$	$5.9 \times 10^{23}$	$3.4 \times 10^{24}$
		85	$5.0 \times 10^{27}$	2.9				$6.1 \times 10^{23}$
		150	$7.0 \times 10^{26}$	0.63				$5.9 \times 10^{23}$
	1/2	50	$2.3 \times 10^{27}$	1.4	43	0.15	$1.3 \times 10^{25}$	$1.8 \times 10^{25}$
		85	$1.2 \times 10^{27}$	0.71				$1.3 \times 10^{25}$
		150	$4.4 \times 10^{26}$	0.38				$1.3 \times 10^{25}$
	1	50	$1.6 \times 10^{27}$	1	32	1	$7.9 \times 10^{25}$	$8.1 \times 10^{25}$
		85	$1.7 \times 10^{27}$	1				$7.9 \times 10^{25}$
		150	$1.1 \times 10^{27}$	1				$7.9 \times 10^{25}$
4.02	1/3	85	$7.7 \times 10^{27}$	2.5	61	$3.8 \times 10^{-3}$	$5.4 \times 10^{23}$	$5.6 \times 10^{23}$
		150	$3.4 \times 10^{27}$	1.6				$5.4 \times 10^{23}$
		300	$6.3 \times 10^{26}$	0.47				$5.4 \times 10^{23}$
	1/2	85	$2.4 \times 10^{27}$	0.77	42	0.13	$1.7 \times 10^{25}$	$1.7 \times 10^{25}$
		150	$1.1 \times 10^{27}$	0.49				$1.7 \times 10^{25}$
		300	$6.1 \times 10^{26}$	0.46				$1.7 \times 10^{25}$
	1	85	$3.2 \times 10^{27}$	1	31	1	$1.1 \times 10^{26}$	$1.1 \times 10^{26}$
		150	$2.1 \times 10^{27}$	1				$1.1 \times 10^{26}$
		300	$1.3 \times 10^{27}$	1				$1.1 \times 10^{26}$

Table 3: Droplet formation rate  $I/V$  (reduced by the system volume) and carrier gas effect  $\mathcal{G}$  from YM canonical ensemble MD simulation as well as the critical droplet size  $\mathcal{N}_{\text{PE}}^*$  (in molecules), the normalized Wedekind et al. (2008) pressure effect  $\mathcal{W}$ , the nucleation rate  $j_{\text{PE}}$  and the droplet formation rate  $j/Q_{\text{PE}}$  (reduced by the volume) according to the PE variant of CNT, in dependence of the supersaturation  $S$  and the mole fraction of  $\text{CO}_2$  in the vapour  $Y_0$  as well as the YM threshold size  $M$  (in molecules) at a temperature of  $T = -44.8$  °C.

of the nucleation rate on the carrier gas density.

While this qualitatively confirms CNT with the pressure effect, which leads to  $\mathcal{W}$  factors on the order of 0.1 for  $Y_0 = 1/2$  and 0.01 for  $Y_0 = 1/3$ , the actual decrease of  $I$  approaches the range 0.3 to 0.4 in the limit of large threshold sizes for both values of  $Y_0$ . This impression consolidates itself if the results for  $T = -34.8$  and  $-23$  °C are also regarded, cf. Fig. 3 and Tab. 4. The normalized Wedekind et al. (2008) pressure effect  $\mathcal{W}$ , corresponding to the deviation between  $j_{\text{PE}}(Y_0)$  and  $j_{\text{PE}}(Y_0 = 1)$ , decreases even faster with  $Y_0 \rightarrow 0$  at high temperatures. Qualitatively, this is confirmed by simulation results, e.g. no nucleation at all was detected at these temperatures for  $Y_0 = 1/3$ , which implies  $j < 10^{25} \text{ cm}^{-3}\text{s}^{-1}$ . However, from the available results for  $Y_0 = 1/2$  it is evident that the pressure effect is overestimated by CNT, in particular at  $T = -23$  °C.

$T$ [°C]	$S$	$Y_0$	$M$	$I/V$ [cm <sup>-3</sup> s <sup>-1</sup> ]	$\mathcal{G}$	$N_{PE}^*$	$\mathcal{W}$	$j_{PE}$ [cm <sup>-3</sup> s <sup>-1</sup> ]	$j/Q_{PE}$ [cm <sup>-3</sup> s <sup>-1</sup> ]	
-34.8	2.80	1/2	50	$1.5 \times 10^{27}$	2.7	66	0.03	$2.9 \times 10^{24}$	$2.6 \times 10^{25}$	
			85	$1.6 \times 10^{26}$	0.76			$3.3 \times 10^{24}$		
	1	50	50	$5.6 \times 10^{26}$	1	41	1	$7.6 \times 10^{25}$	$9.9 \times 10^{25}$	
			85	$2.1 \times 10^{26}$	1			$7.6 \times 10^{25}$		
	3.08	1/2	50	$5.5 \times 10^{27}$	9.5	65	0.02	$3.9 \times 10^{24}$	$3.1 \times 10^{25}$	
			150	$3.1 \times 10^{26}$	1.0			$3.9 \times 10^{24}$		
	1	50	50	$6.3 \times 10^{27}$	1	39	1	$1.3 \times 10^{26}$	$1.6 \times 10^{26}$	
			150	$2.9 \times 10^{26}$	1			$1.3 \times 10^{26}$		
	3.36	1/3	n/a		$< 10^{25}$	$< 0.01$	127	$4.2 \times 10^{-6}$	$1.1 \times 10^{21}$	n/a
			1/2	50	$1.1 \times 10^{28}$	1.6	65	0.02	$4.2 \times 10^{24}$	$8.7 \times 10^{24}$
		1	300	$3.2 \times 10^{26}$	0.22			$4.2 \times 10^{24}$		
			50	$6.7 \times 10^{27}$	1	37	1	$1.8 \times 10^{26}$	$2.1 \times 10^{26}$	
300	$1.4 \times 10^{27}$	1			$1.8 \times 10^{26}$					
-23.0	2.34	1/2	50	$1.1 \times 10^{28}$	8.5	140	$1.9 \times 10^{-4}$	$4.0 \times 10^{22}$	$1.8 \times 10^{27}$	
			100	$1.1 \times 10^{27}$	3.3			$7.8 \times 10^{23}$		
	1	50	50	$1.3 \times 10^{27}$	1	54	1	$1.4 \times 10^{26}$	$3.9 \times 10^{26}$	
			100	$3.4 \times 10^{26}$	1			$1.4 \times 10^{26}$		
	2.53	1/2	85	$7.4 \times 10^{27}$	3.4	143	$1.0 \times 10^{-4}$	$3.0 \times 10^{22}$	$3.9 \times 10^{24}$	
			200	$7.4 \times 10^{26}$	0.96			$3.1 \times 10^{22}$		
	1	85	85	$2.2 \times 10^{27}$	1	52	1	$1.9 \times 10^{26}$	$1.9 \times 10^{26}$	
			200	$7.7 \times 10^{26}$	1			$1.9 \times 10^{26}$		
	2.72	1/3	n/a		$< 10^{25}$	$< 0.01$	879	$4.3 \times 10^{-25}$	$2.3 \times 10^2$	n/a
			1/2	75	$1.3 \times 10^{28}$	2.6	150	$4.2 \times 10^{-5}$	$1.7 \times 10^{22}$	$1.8 \times 10^{25}$
		1	250	$1.6 \times 10^{27}$	1.1			$1.7 \times 10^{22}$		
			75	$4.8 \times 10^{27}$	1	50	1	$2.5 \times 10^{26}$	$2.6 \times 10^{26}$	
250	$1.4 \times 10^{27}$	1			$2.5 \times 10^{26}$					

Table 4: Droplet formation rate  $I/V$  (reduced by the system volume) and carrier gas effect  $\mathcal{G}$  from YM canonical ensemble MD simulation as well as the critical droplet size  $N_{PE}^*$  (in molecules), the normalized Wedekind et al. (2008) pressure effect  $\mathcal{W}$ , the nucleation rate  $j_{PE}$  and the droplet formation rate  $j/Q_{PE}$  (reduced by the volume) according to the PE variant of CNT, in dependence of temperature  $T$ , supersaturation  $S$  and the mole fraction of CO<sub>2</sub> in the vapour  $Y_0$  as well as the YM threshold size  $M$  (in molecules).

## 5. Conclusion

Vapour-liquid coexistence in equilibrium and non-equilibrium was studied by molecular simulation for systems consisting of CO<sub>2</sub>, N<sub>2</sub>, O<sub>2</sub>, and Ar. For the nucleation of pure CO<sub>2</sub>, it was found that the simplified classical variant of CNT and the variant of CNT which takes the pressure effect into account both underestimate the nucleation rate. This deviation can reach a factor 20 for the simplified variant and varies between one and three orders of magnitude if the pressure effect is considered.

It should be noted that this result for pure CO<sub>2</sub> nucleation is both qualitatively and quantitatively similar to the deviation of CNT for homogeneous nucleation of the truncated-shifted LJ fluid (Horsch et al., 2008b). In that case, it was shown that the deviation can be corrected by a thermo-

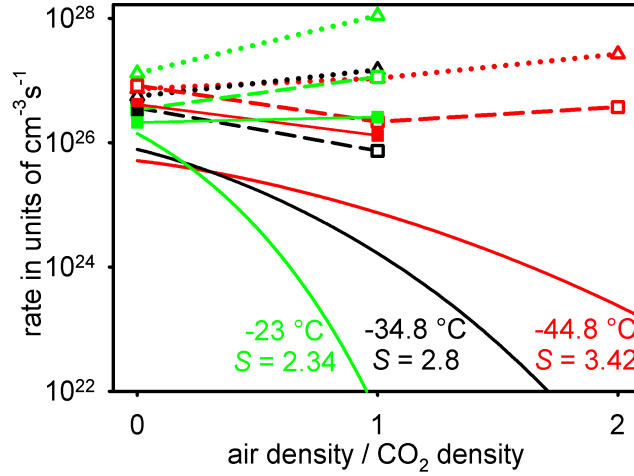


Figure 3: (Colour on the web and in print.) Nucleation rate  $j_{PE}$  according to CNT with the pressure effect in comparison to  $I/V$  for threshold sizes of  $M = 50$  ( $\Delta \cdots \Delta$ ),  $100$  ( $\square - - \square$ ), and  $150$  ( $\bullet - - \bullet$ ) molecules from canonical ensemble MD simulation in dependence of  $Y_0^{-1} - 1$ , i.e. the ratio between air and  $\text{CO}_2$  molecules in the system, for  $T = -44.8$  °C with  $S = 3.42$  and  $T = -34.8$  °C with  $S = 2.8$  as well as  $T = -23$  °C with  $S = 2.34$ . Note that in the latter two cases, no nucleation was detected during the MD simulation run for  $Y_0^{-1} - 1 = 1$  and  $2$ , implying that  $I/V < 10^{25} \text{ cm}^{-3} \text{ s}^{-1}$ .

dynamically consistent approach that takes both the curvature dependence of  $\gamma$  and the increased surface area due to fluctuations of the droplet geometry into account. Future work could elaborate on that and validate whether a theory based on these considerations, e.g. as expressed by Eqs. (18) and (19), applies for  $\text{CO}_2$  as well.

The effect of air as a carrier gas on  $\text{CO}_2$  nucleation as determined from MD simulation qualitatively confirms the theory outlined by Wedekind et al. (2008). Although significant quantitative deviations were found, these are partly due to the fact that at the high densities corresponding to the present simulations, air cannot be reliably described by the ideal gas equation. The non-ideality leads to a lower total pressure and thereby reduces the magnitude of the pressure effect to a certain extent.

## Acknowledgements

The authors would like to thank M. Bernreuther (Stuttgart) for his valuable support regarding organisational and technical issues, D. Reguera López and J. Wedekind (Barcelona), G. Chkonia and J. Wölk (Cologne), G. Guevara Carrión and J. Walter (Kaiserslautern) as well as Y.-L. Huang and S. Miroshnichenko (Paderborn) for raising interest in the subject and for lively discussions, and the Federal Ministry of Education and Research (BMBF) for funding the project IMEMO. The presented research was carried out under the auspices of the Boltzmann-Zuse Society of Computational Molecular Engineering (BZS), and the simulations were performed on the Opteron cluster *phoenix* and the NEC Nehalem cluster *laki* at the High Performance Computing Center Stuttgart (HLRS) under the grant MMHBF.

## Literature

- Bernreuther, M., Niethammer, C., Horsch, M., Vrabec, J., Deublein, S., Hasse, H., Buchholz, M., 2009. Innovative HPC methods and application to highly scalable molecular simulation. *Innovatives Supercomputing in Deutschland* 7 (1): 50–53.
- Berthelot, D., 1898. Sur le mélange des gaz. *Comptes rendus hebdomadaires des séances de l'Académie des Sciences* 126, 1703–1706, 1857–1858.
- Blander, M., Katz, J. L., 1972. The thermodynamics of cluster formation in nucleation theory. *Journal of Statistical Physics* 4 (1), 55–59.
- Brus, D., Hyvärinen, A.-P., Wedekind, J., Viisanen, Y., Kulmala, M., Ždímal, V., Smolík, J., Lihavainen, H., 2008. The homogeneous nucleation of 1-pentanol in a laminar flow diffusion chamber: The effect of pressure and kind of carrier gas. *The Journal of Chemical Physics* 128, 134312.
- Chesnokov, E. N., Krasnoperov, L. N., 2007. Complete thermodynamically consistent kinetic model of particle nucleation and growth: Numerical study of the applicability of the classical theory of homogeneous nucleation. *The Journal of Chemical Physics* 126, 144504.
- Chkonia, G., Wölk, J., Strey, R., Reguera, D., 2009. Evaluating nucleation rates in direct simulations. *The Journal of Chemical Physics* 130, 064505.
- Dodge, B. F., 1927. *Chemical & Metallurgical Engineering* 10, 622.
- Feder, J., Russell, K. C., Lothe, J., Pound, G. M., 1966. Homogeneous nucleation and growth of droplets in vapours. *Advances in Physics* 15 (1), 111–178.
- Gray, C. G., Gubbins, K. E., 1984. *Theory of molecular fluids, Volume 1: Fundamentals*. Clarendon, Oxford.
- Hopcroft, J., Tarjan, R., 1973. Efficient algorithms for graph manipulation. *Communications of the ACM* 16 (6): 372–378.
- Horsch, M., Miroshnichenko, S., Vrabec, J., 2009. Steady-state molecular dynamics simulation of vapour to liquid nucleation with McDonald's daemon. *Journal of Physical Studies (L'viv)*, in press; arXiv: 0911.5485v1 [physics.aoph]. URL <http://arXiv.org/abs/0911.5485>.
- Horsch, M., Vrabec, J., 2009. Grand canonical steady-state simulation of nucleation. *The Journal of Chemical Physics* 131, 184104.
- Horsch, M., Vrabec, J., Bernreuther, M., Grottel, S., Reina, G., Wix, A., Schaber, K., Hasse, H., 2008a. Homogeneous nucleation in supersaturated vapors of methane, ethane, and carbon dioxide predicted by brute force molecular dynamics. *The Journal of Chemical Physics* 128, 164510.
- Horsch, M., Vrabec, J., Hasse, H., 2008b. Modification of the classical nucleation theory based on molecular simulation data for surface tension, critical nucleus size, and nucleation rate. *Physical Review E* 78, 011603.
- Huang, Y.-L., Vrabec, J., Hasse, H., 2009. Prediction of ternary vapor-liquid equilibria for 33 systems by molecular simulation. *Fluid Phase Equilibria* 287, 62–69.
- Hyvärinen, A.-P., Brus, D., Ždímal, V., Smolík, J., Kulmala, M., Viisanen, Y., Lihavainen, H., 2006. The carrier gas pressure effect in a laminar flow diffusion chamber, homogeneous nucleation of *n*-butanol in helium. *The Journal of Chemical Physics* 124, 224304, erratum: 2008; *The Journal of Chemical Physics* 128, 109901.
- Iland, K., Wedekind, J., Wölk, J., Wagner, P. E., Strey, R., 2004. Homogeneous nucleation rates of 1-pentanol. *The Journal of Chemical Physics* 121 (24), 12259–12264.
- Kaule, G., 2002. *Umweltplanung*. Eugen Ulmer, Stuttgart.
- Lorentz, H. A., 1881. Ueber die Anwendung des Satzes vom Virial in der kinetischen Theorie der Gase. *Annalen der Physik (Leipzig)* 12 (1), 127–136, addendum: 1881; *Annalen der Physik (Leipzig)* 12(4), 660–661.
- Määttänen, A., Vehkamäki, H., Lauri, A., Merikallio, S., Kauhanen, J., Savijärvi, H., Kulmala, M., 2005. Nucleation studies in the Martian atmosphere. *Journal of Geophysical Research E – Planets* 110, 02002.
- Matsubara, H., Koishi, T., Ebisuzaki, T., Yasuoka, K., 2007. Extended study of molecular dynamics simulation of homogeneous vapor-liquid nucleation of water. *The Journal of Chemical Physics* 127, 214507.
- Moody, M. P., Attard, P., 2003. Curvature-dependent surface tension of a growing droplet. *Physical Review Letters* 91 (5).
- Nellas, R. B., Chen, B., Siepmann, J. I., 2007. Dumbbells and onions in ternary nucleation. *Physical Chemistry Chemical Physics* 9, 2779–2781.
- Schnabel, T., Srivastava, A., Vrabec, J., Hasse, H., 2007a. Hydrogen bonding of methanol in supercritical CO<sub>2</sub>:

- Comparison between  $^1\text{H}$ -NMR spectroscopic data and molecular simulation results. *Journal of Physical Chemistry B* 111, 9871–9878.
- Schnabel, T., Vrabec, J., Hasse, H., 2007b. Unlike Lennard-Jones parameters for vapor-liquid equilibria. *Journal of Molecular Liquids* 130, 170–178.
- Stillinger, F. H., 1963. Rigorous basis of the Frenkel-Band theory of association equilibrium. *The Journal of Chemical Physics* 38 (7), 1486–1494.
- Strey, R., Viisanen, Y., 1993. Measurement of the molecular content of binary nuclei. Use of the nucleation rate surface for ethanol–hexanol. *The Journal of Chemical Physics* 99 (6), 4693–4704.
- Strey, R., Viisanen, Y., Wagner, P. E., 1995. Measurement of the molecular content of binary nuclei. 3. Use of the nucleation rate surfaces for the water-*n*-alcohol series. *The Journal of Chemical Physics* 103 (10), 4333–4345.
- Suehiro, Y., Nakajima, M., Yamada, K., Uematsu, M., 1996. Critical parameters of  $x \text{CO}_2 + (1 - x)\text{CHF}_3$  for  $x = 1.0000, 0.7496, 0.5013, \text{ and } 0.2522$ . *The Journal of Chemical Thermodynamics* 28: 1153–1164.
- Szybisz, L., Urrutia, I., 2003. Curvature effects on the surface thickness and tension at the free interface of  $^4\text{He}$  systems. *Physical Review B* 68, 054518.
- Tolman, R. C., 1949. The effect of droplet size on surface tension. *The Journal of Chemical Physics* 17 (3), 333–337.
- Valeriani, C., Sanz, E., Frenkel, D., 2005. Rate of homogeneous crystal nucleation in molten NaCl. *The Journal of Chemical Physics* 122, 194501.
- Viisanen, Y., Strey, R., Laaksonen, A., Kulmala, M., 1994. Measurement of the molecular content of binary nuclei. 2. Use of the nucleation rate surface for water-ethanol. *The Journal of Chemical Physics* 100 (8), 6062–6072.
- Vrabec, J., Hasse, H., 2002. Grand Equilibrium: Vapour-liquid equilibria by a new molecular simulation method. *Molecular Physics* 100, 3375–3383.
- Vrabec, J., Huang, Y.-L., Hasse, H., 2009a. Molecular models for 267 binary mixtures validated by vapor-liquid equilibria: A systematic approach. *Fluid Phase Equilibria* 279 (2), 120–135.
- Vrabec, J., Kedia, G. K., Buchhauser, U., Meyer-Pitroff, R., Hasse, H., 2009b. Thermodynamic models for vapor-liquid equilibria of nitrogen + oxygen + carbon dioxide at low temperatures. *Cryogenics* 49, 72–79.
- Vrabec, J., Stoll, J., Hasse, H., 2001. A set of molecular models for symmetric quadrupolar fluids. *Journal of Physical Chemistry B* 105 (48), 12126–12133.
- Wedekind, J., Chkonia, G., Wölk, J., Strey, R., Reguera, D., 2009. Crossover from nucleation to spinodal decomposition in a condensing vapor. *The Journal of Chemical Physics* 131: 114506.
- Wedekind, J., Hyvärinen, A.-P., Brus, D., Reguera, D., 2008. Unraveling the ‘Pressure Effect’ in nucleation. *Physical Review Letters* 101, 125703.
- Yasuoka, K., Matsumoto, M., 1998. Molecular dynamics of homogeneous nucleation in the vapor phase. *The Journal of Chemical Physics* 109 (19), 8451–8470.
- Zěl’dovič, Ā. B., 1942. K tēorii obrazovaniā novoī fazy. Kavitaciā. *Žurnal Eksperimental’noī i Teoreticheskoī Fiziki* 12, 525–538.